Railway Engineering Science
https://doi.org/10.1007/s40534-026-00441-8

Development of a modelling framework for running safety analysis of a heavy-haul freight vehicle crossing a bridge under different loading conditions

Eduardo C. Granato[1] · **Gonçalo Ferreira**[2,3] · **Pedro Montenegro**[2] · **Túlio N. Bittencourt**[1]

Received: 14 November 2025 / Revised: 12 April 2026 / Accepted: 14 April 2026
© The Author(s) 2026

Abstract
Evaluation of train running safety for freight and heavy-haul railway vehicles is a poorly addressed topic in the literature, despite their distinct dynamic behaviour and track conditions compared with passenger and high-speed railways. For this purpose, a framework for the development of a three-dimensional numerical analysis of train running safety crossing a bridge using a vehicle–structure interaction methodology is presented. Numerical models of the railway bridge were developed and calibrated, and multibody models of the heavy-haul vehicles were created and optimised based on modal data. Structure and vehicle dynamic responses were obtained using the dynamic interaction models that consider nonlinear wheel–rail contact models. Assessment of structural and train running safety was performed for multiple train speeds for both loaded and unloaded vehicles using different degrees of rail geometric irregularities based on the Federal Railroad Administration's power spectral density functions. The case study is a 550-metre-long railway bridge composed of 22 simply supported steel-concrete composite spans, crossed by heavy-haul vehicles of the gondola-type wagon with 375 kN axle loads. The safety of the bridge was assessed in terms of structural responses according to European codes, while the running safety of the vehicle was evaluated through indirect running safety indices as well as direct derailment coefficients based on vertical and lateral wheel–rail contact forces and more advanced criteria. It was found that in regular operational conditions, all indices are well below recommended limit values for loaded vehicles, whereas the unloaded vehicles presented a more unstable dynamic behaviour.

Keywords Train running safety · Vehicle–structure interaction · Railway bridges · Heavy-haul vehicle

1 Introduction

In freight railway bridges designed for heavy-haul trains, dynamic phenomena play a significant role due to the regular repetition of axles, high loads, and the presence of a considerable degree of track irregularities. Due to this, bridges can experience high dynamic impact forces, a high degree of vibrations and even the possibility of the occurrence of resonance, which may lead to structure and track damage or unsafe conditions for traffic. Thus, it is essential to employ methodologies to design and assess bridge structures not only from the structural safety point of view but also considering the safety of the trains crossing it. Since both the bridge and vehicles crossing it are dynamic systems, their behaviour influences each other, creating a complex dynamic problem that requires specific modelling techniques and dynamic methodologies for its solution.

✉ Eduardo C. Granato
ecgranato@usp.br

Gonçalo Ferreira
gcferreira@fe.up.pt

Pedro Montenegro
paires@fe.up.pt

Túlio N. Bittencourt
tbitten@usp.br

[1] Department of Structural and Geotechnical Engineering, University of São Paulo, Av. Prof. Almeida Prado, Trav. do Biênio, 83, São Paulo 05508-070, São Paulo, Brazil

[2] CONSTRUCT, Faculty of Engineering, University of Porto, Rua Dr. Roberto Frias, 4200-465 Porto, Portugal

[3] RAIL CoLAB, Rua do Ferroviário, 4460-020 Guifões, Portugal

Published online: 08 July 2026

Dynamic assessment of the structure and vehicle responses is essential to ensure structural and running safety in regular or extreme operational conditions, where a dynamic interaction model is necessary. While bridge structures may be accurately represented using conventional commercial finite element modelling software, these do not possess integrated modules to solve dynamic interaction problems or wheel-rail interface representations. On the other hand, commercial vehicle design and assessment software, such as SIMPACK®, VAMPIRE®, ADAMS/RAIL® or NUCARS®, can accurately represent the vehicle behaviour through multibody models and precise wheel-rail contact models, but do not include the tools to model bridges or complex structures, relying solely on track models. Thus, specific methods must be developed and implemented to solve this complex problem.

Modelling techniques for vehicle, track and bridge subsystems are extensively discussed in the literature, such as the review by Cantero et al. [1], the important aspects of train-track-bridge interaction given by Zhai et al. [2], and the discussion on the external excitations to which these systems are subjected by Li et al. [3]. These are of great importance in understanding the challenge of modelling all the interacting subsystems, as well as the solution of the coupled problem. Furthermore, accurate representation of the wheel-rail contact problem is of utmost importance to properly characterise the vehicle's dynamic behaviour, especially in extreme situations where flange impacts and other nonlinear events are expected. Extensive discussions of wheel-rail contact models can be observed in Jin et al. [4], while an example of development and validation can be found in Montenegro et al. [5]. Using these methods, it is possible to calculate the wheel-rail contact forces and relative displacements, which allow for a detailed description of the vehicle behaviour even under extreme conditions, calculation of derailment indices and development of running safety evaluations.

Vehicle–structure interaction and train running safety assessments have had an increasing focus in the literature in recent decades due to the importance of guaranteeing traffic safety and maintaining infrastructure quality, which was initially led by the rapid development of high-speed railways. Authors tend to investigate different scenarios where running safety may be harmed, such as the work by Yang and Yau [6] where vehicle resonance caused by interaction with a series of simply supported or continuous beams was studied, or the study by Ribeiro et al. [7] where the behaviour of a centenary metallic bridge subject to metro traffic was evaluated. Furthermore, many researchers use vehicle–structure interaction methodologies to establish safety criteria, such as the work by Arvidsson et al. [8], which investigates the bridge deck acceleration criteria from a running safety point of view, the study of the dynamic amplification factors due to high-speed traffic by Ma et al. [9], or the additional damping effects observed when considering vehicle-bridge interaction discussed by Stoura and Dimitrakopoulos [10].

Furthermore, many works investigate train running safety considering external excitations which may significantly harm vehicle stability, such as works by Wang et al. [11] and Montenegro et al. [12], where the effects of crosswinds are investigated, and by Gong et al. [13] and Zhao et al. [14], that study running safety under ground motion actions. Nevertheless, most studies still remain focused on high-speed trains, which are naturally more susceptible to instabilities due to their high operational speed, relatively low mass and real possibilities of causing resonance.

For heavy-haul operations, however, the challenges shift towards different dynamic effects caused by heavy axle loads operating at lower speeds, and the design of track components and substructure will reflect these distinct characteristics, as demonstrated by Giannakos [15]. Unlike typical passenger and high-speed rail lines, where the design and maintenance needs are focused on maintaining extremely tight geometric tolerances, freight lines tend to prioritise track stiffness and fatigue resistance, as discussed by Esveld [16] and Li et al. [17]. Furthermore, Selig and Waters [18] also show that the types of damage expected from regular operation in heavy-haul lines are associated with plastic deformations of the subgrade or track structure, which will inevitably lead to different monitoring and maintenance needs.

Track quality standards have been extensively discussed in the literature in works by El-Sibaie and Zhang [19] and Zhao et al. [20], for example. Technical recommendations are also found in several guidelines, such as those published by the International Union of Railways (UIC) [21, 22], and Andrade and Teixeira [23] discussed differentiation between passenger and freight traffic as that proposed by the UIC [24]. Thus, it is known that for freight and heavy-haul rail lines, other types of issues that are not common in conventional or high-speed passenger transport may be observed due to different operational conditions and maintenance standards, which may lead to unforeseen traffic hazards. These would be mostly related to track quality deterioration and exaggerated structural deformations, which must be properly modelled and evaluated to ensure running safety.

Investigations in freight and heavy-haul railways tend to explore the dynamic responses of bridges in the face of increased loads, as discussed by Ticona Melo et al. [25], as well as the effects of train formation numbers, which were investigated by Xiao et al. [26]. Research on this type of rail vehicle is much less prevalent than passenger traffic in the literature, especially in terms of running safety, which may be critical in certain situations. Freight and heavy-haul rail vehicles are notoriously less stable due to their single-stage suspensions with high stiffness, leading to a lesser capability of adapting to worse track conditions, which may be amplified in the unloaded conditions without the high mass stabilising effects. Furthermore, track conditions may be worse due to different maintenance standards and typical damage observed in heavy-haul lines, leading to high degrees of vertical and lateral excitations.

To address these challenges, this paper aims to present a framework developed to model and investigate the running safety of heavy-haul trains using a three-dimensional vehicle–structure interaction model with nonlinear wheel-rail contact models. A thorough evaluation of structural and vehicle behaviour is performed in a bridge used in a heavy-haul railway line, both in the loaded and unloaded vehicle configurations under different degrees of track irregularities. For this, the methods used are described in Sect. 2, where in Sect. 2.1, the methodology used to solve the vehicle–structure interaction problem is presented along with a description of the wheel-rail contact in Sect. 2.2. The methods and criteria used for the evaluation of train running safety are given in Sect. 2.3. In Sect. 3, the techniques used to develop and calibrate the numerical models of the vehicle and structure are described. Finally, the dynamic results of the analysis of the case study are given in Sect. 4 and systematic safety analyses for all modelling scenarios are presented in Sect. 4.3, with concluding remarks given in Sect. 5.

2 Methods

2.1 Vehicle–structure interaction

Train-track-bridge coupled systems are complex dynamic systems, where the behaviour of each of the subsystems influences the others, leading to the necessity of solving all subsystems simultaneously. For this, multiple methodologies can be used, either considering the vehicle and structures separately and establishing their coupling iteratively or defining additional constraint equations and solving the whole system simultaneously. In this work, a vehicle–structure interaction (VSI) algorithm named direct method was used, originally proposed by Neves et al. [27] and later extended by Montenegro et al. [28] to account for the lateral interaction. This methodology was employed to calculate the structure and vehicle responses based on a three-dimensional analysis with consideration of nonlinear wheel-rail contact. The dynamic interaction solution method is based on the Lagrange multiplier method, which creates a coupled global matrix of the two systems, namely the vehicle and track–structure systems. The coupling between wheel and rail nodes is represented through additional constraint equations that establish the displacement relations in the contact points, forming a single system of equations.

The equilibrium equations of a vehicle–structure dynamic system can be written according to the α method and are given in Eq. (1), where $\boldsymbol{M}$ is the mass matrix, $\boldsymbol{R}$ is the internal node force vector, $\boldsymbol{F}$ is the vector of external loads and $\boldsymbol{a}$ is the nodal displacement vector, t and $t+\Delta t$ are the previous and current time step, respectively, and α is the α method constant.

$$\boldsymbol{M}\ddot{\boldsymbol{a}}^{t+\Delta t} + (1+\alpha)\boldsymbol{R}^{t+\Delta t} - \alpha \boldsymbol{R}^{t} = (1+\alpha)\boldsymbol{F}^{t+\Delta t} - \alpha \boldsymbol{F}^{t}. \tag{1}$$

The development of the equations of equilibrium using the iterative Newton method for the solution of the nonlinear system, which is not given herein for brevity, leads to the final system of equations that is given in Eq. (2). In this equation, $\overline{\boldsymbol{K}}$ is the effective stiffness matrix, $\overline{\boldsymbol{D}}$ is the transformation matrix that relates the contact forces with nodal forces in the structure, and vectors Δa and ΔX are the incremental nodal displacements and contact forces, $\boldsymbol{\psi}$ is the residual force vector resultant from the nonlinear wheel–rail contact problem, and i and $i+1$ indicate the previous and current iterations, respectively. For a more detailed step-by-step solution, we refer the reader to Montenegro et al.'s work [28].

$$\begin{bmatrix} \overline{\boldsymbol{K}}\, \boldsymbol{D} \end{bmatrix} \begin{bmatrix} \Delta a_F^{t+\Delta t, i+1} \\ \Delta X_F^{t+\Delta t, i+1} \end{bmatrix} = \boldsymbol{\psi}(\boldsymbol{a}^{t+\Delta t, i}, \boldsymbol{X}^{t+\Delta t, i}). \tag{2}$$

Constraint equations must also be included to establish compatibility in the displacements of the contact nodes since the contact and target elements are coupled in three directions. This is done following Eq. (3), where $\boldsymbol{v}^{\mathrm{c}}$ and $\boldsymbol{v}^{\mathrm{t}}$ are the displacements of the wheel and rail elements, respectively, and $\boldsymbol{r}$ is the rail irregularity value under the contact node.

$$\boldsymbol{v}^{\mathrm{c}} + \boldsymbol{v}^{\mathrm{t}} = \boldsymbol{r}. \tag{3}$$

The constraint equations thus can be developed to find Eq. (4), where $\overline{\boldsymbol{H}}$ is the matrix that transforms the displacements of the contact nodes from the global to the local coordinate system.

$$\overline{\boldsymbol{H}} \Delta a^{t+\Delta t, i+1} = \overline{\boldsymbol{r}}. \tag{4}$$

Finally, the final system of equations is described in Eq. (5). In this Equation, a single system of equations can be solved simultaneously with displacements and contact forces as unknown variables, completely solving the vehicle–structure interaction problem.

$$\begin{bmatrix} \overline{\boldsymbol{K}} & \overline{\boldsymbol{H}} \\ \overline{\boldsymbol{D}} & 0 \end{bmatrix} \begin{bmatrix} \Delta a_F^{i+1} \\ \Delta X_F^{i+1} \end{bmatrix} = \begin{bmatrix} \boldsymbol{\psi}(\boldsymbol{a}^{t+\Delta t,i}, \boldsymbol{X}^{t+\Delta t,i}) \\ \overline{\boldsymbol{r}} \end{bmatrix}. \tag{5}$$

2.2 Wheel–rail contact modelling

Complex wheel–rail contact models are essential to accurately simulate the dynamic behaviour of railway vehicles, especially in the lateral direction. Typical formulations are based on finding the exact contact point between wheel tread and rail head explicitly and calculating the vertical and lateral contact forces using specific theories. In this work, a methodology proposed by Montenegro et al. [28] and later expanded ([5]) to include possible contact on the concave region of the wheel was used. In this, the wheel–rail contact problem is divided into three parts: i) the geometric contact problem; ii) the normal contact problem, and iii) the tangential contact problem.

In the geometric problem, the parametrised profile surface of the wheel and rail is used using either a convex or concave search algorithm based on the solution of a nonlinear set of equations to detect potential contact points. With this, the properties of the contact surfaces can be obtained, such as the curvature of the surfaces in the contact point, which are used to calculate the contact forces.

In the normal contact problem, the nonlinear Hertz theory [29] is employed to calculate the normal force developed in the compressed region between the two bodies. Using Eq. (6), the normal contact force $F_{\rm n}$ is calculated using the generalised stiffness coefficient $K_{\rm h}$ and d is the penetration found in the geometric contact problem.

$$F_{\rm n} = K_{\rm h} d^{2/3}. \tag{6}$$

Finally, the tangential contact problem is formulated in terms of non-dimensional creepages, defined as the relative velocities between the wheel and rail at the contact point normalised by the vehicle forward speed, following Kalker's rolling contact theory [30]. The resulting longitudinal and lateral creep forces, as well as the spin creep moment, are computed using the USETAB algorithm proposed by Kalker [31]. In this approach, the normalised tangential forces are precalculated and stored in lookup tables as functions of the creepages and the semi-axes ratio of the contact ellipse, and are subsequently interpolated during the dynamic analysis to obtain the tangential contact forces.

Due to space constraints, a description of the mathematical formulation of the VSI tool and wheel-rail contact model employed for vehicle–bridge dynamic interaction analyses is not given in this work. A comprehensive description and extensive validation against both numerical and experimental cases are provided in [5, 28].

2.3 Safety evaluation

Train running safety can be evaluated through direct or indirect methodologies. Due to the complexity of vehicle–structure interaction methods, norms and recommendations often provide alternative approaches to assess vehicle responses and ensure running safety based on indirect indicators, such as bridge responses and properties, either through static or moving loads dynamic analyses. Since no derailment mechanisms are explicitly evaluated, this approach is naturally more conservative and may not represent the complex behaviour of the wheel–rail contact in extreme cases.

On the other hand, train running safety may be assessed explicitly based on the study of the wheel–rail contact forces and the mechanisms that lead to derailment. In this way, it is possible to establish criteria that will guarantee the avoidance of situations where these mechanisms will occur. A comprehensive description of such mechanisms and criteria is not given herein due to space constraints. However, for an in-depth analysis of derailment mechanisms, running safety assessment techniques and normative recommendations for bridge response limits, the reader is referred to Montenegro et al.'s review on train running safety assessment [32].

Among the most commonly used running safety criteria are the Nadal [33], Prud'Homme [34] and wheel unloading criteria, which are described along with limit values and references in Table 1 and pictured in Fig. 1, where Y and Q are the lateral and vertical dynamic wheel-rail contact forces, respectively, and Q_0 is the static load. Limit values can be found in codes and recommendations, such as EN 14067 [35] and EN 14363 [36], AAR [37] or others, and must be carefully considered depending on the scope and applications. In this work, the values given in Table 1 will be considered for reference.

With a more detailed and less conservative approach, analyses can be performed to verify that derailment will only occur after the flange height has been surpassed by the wheel-rail relative displacement. For this, criteria have been proposed in the literature which associate the exceedance of thresholds for certain periods of time, such as the works by Ishida and Matsuo [38] and Ishida et al. [39] that consider the time of 15 ms for the Y/Q ratio. The same criterion is

Table 1 Summary of safety criteria adopted

Bridge responses				
Direction	Response	Limit value	Unit	Reference
Vertical	Displacement	$L/600$	m	[41]
	Acceleration	3.5	m/s^2	[41]
Vehicle responses				
Direction	Response	Limit value	Unit	Reference
Vertical	Acceleration	5.0	m/s^2	[21]
Lateral		3.0	m/s^2	[21]
Derailment				
Mechanism	Criterion	Coefficient	Limit value	Reference
Flange climbing	Nadal	$\zeta_{\mathrm{N}} = \frac{Y}{Q}$	0.8	[42]
Panel shift	Prud'homme	$\zeta_{\mathrm{P}} = \frac{\sum_{\mathrm{WS}} Y}{10+2Q_0/3}$	1.0	[42]
Wheel unloading	Unloading	$\zeta_{\mathrm{U}} = \frac{\Delta Q}{Q_0}$	0.9	[37]

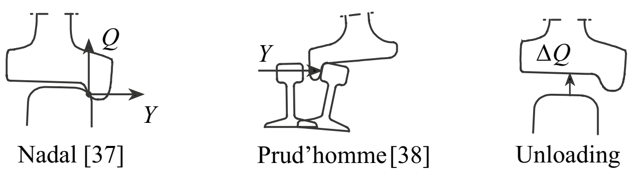

Fig. 1 Derailment mechanisms and running safety criteria

also discussed by Montenegro [40], who demonstrates how conservative these values can be. Arvidsson et al. [8] also extend the duration limit for the unloading coefficient, discussing that short-time wheel unloading, characteristic of high-frequency oscillations, is not relevant for derailment due to the small rise of the wheel during these loss-of-contact situations. Thus, the authors propose using the same 15 ms criterion for the contact loss occurrences, in line with the studies mentioned earlier for the flange climbing mechanisms. With a similar approach, the AAR [37] discusses that failure may be defined if the limit values established for the coefficients are surpassed for 50 ms or a distance of 3 feet.

It is noteworthy to mention that many of the recommendations concerning safety and running behaviour of rolling stock are prepared for testing and approval of railway vehicles [21, 36]. As such, these codes present strict requirements concerning their dynamic behaviour that must be followed by vehicles to be accepted into service. With this in mind, it is expected that some of these criteria to be conservative and their use to evaluate safety in field service conditions should be done carefully.

3 Modelling

The coupled nature of the vehicle–structure interaction problem requires the modelling of all subsystems to assess the complete behaviour of the train–track–bridge system. However, since the solution of coupled systems is extremely computationally intensive, the numerical models should achieve a compromise between accuracy and computational efficiency. For running safety analyses, the most common approach is to use simplified frame models for the bridge and multibody models for the vehicle, which can accurately represent the whole coupled system for contact force calculation and, consequently, running safety indices. In the following subsections, the modelling strategies for the bridge, track and vehicle models are discussed.

3.1 Structure

The structure in this case study consists of 22 simply supported steel-concrete composite spans of 25 metres each, crossing a valley with 30-m-high piers at the highest points. The deck can be described as a composite structure with two 2.4 metres-high steel beams with vertical and horizontal web stiffeners, bracing of the top flanges, and bracing on the bottom horizontal plane using diagonals and in the vertical plane using K-type intermediate bracing frames spaced roughly every 5 metres. The concrete deck is a reinforced concrete slab 30 centimetres thick. All piers have the same hollow rectangular cross-section with dimensions of 3.0 by 5.5 m and 30-cm-thick walls (Fig. 2).

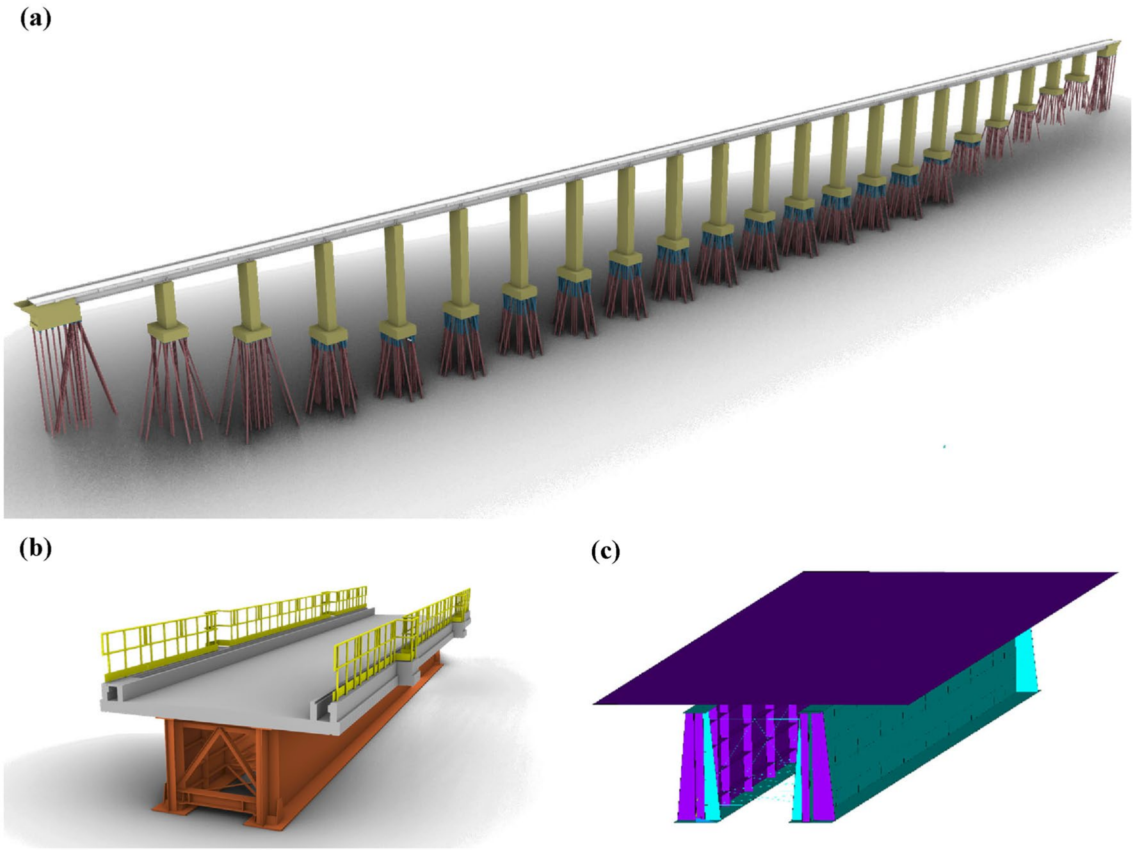

Fig. 2 Three-dimensional models of the studied bridge: **a** longitudinal view of the bridge; **b** view of the deck; **c** finite element model

In order to achieve better computational efficiency, the bridge deck was modelled using spatial frame elements of the homogenised steel-concrete composite deck, whose properties were calculated based on the geometry and mechanical properties of the steel beams and concrete slabs. Furthermore, a complex three-dimensional shell model of the bridge was also developed to calibrate and validate the results from the simplified frame element using modal and dynamic analyses with a moving loads methodology based on the vertical responses of the deck. A dynamic analysis with moving loads representing the loaded wagon models that are described in Sect. 3.3 at the speed of 80 km/h was conducted, and the results for midspan accelerations and displacements from both models are given in Fig. 3, where it is clear that both models produce remarkably similar results with less than 5% difference on the displacements at its highest. The slightly higher vertical stiffness in the refined model is attributed to the overall stiffer behaviour of the shell elements and the complete modelling of all bracing structural elements, which were not considered in the homogenised frame model.

The final properties of the frame element are given in Table 2, where the properties are those used to define the BEAM188 element of ANSYS software, namely the area, moment of inertia about the y axis, product of inertia, moment of inertia about the z axis, warping constant, torsional constant, coordinates of centroid on the the y and z axes, coordinates of the shear centre in the y and z axis, and thickness along z axis, respectively, all with units following the SI.

Once the numerical models were constructed, modal analyses were conducted to characterise their dynamic behaviour. The refined deck model, with its detailed shell

Table 2 Properties of the equivalent beam cross-section

A (m^2)	I_{yy} (m^4)	I_{yz} (m^4)	I_{zz} (m^4)	I_w (m^6)	J (m^4)	z_{gc} (m)	y_{cg} (m)	SH_y (m)	SH_z (m)	TK_z (m)
0.437	0.447	0.1	1.083	1.0	1.0	1.914	0.0	0.0	2.789	6.0

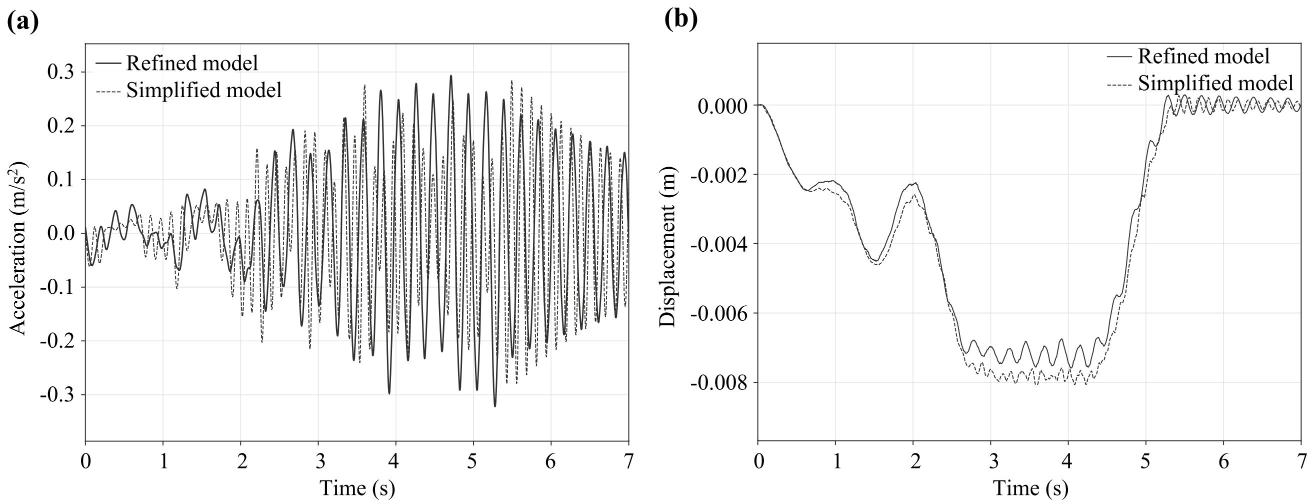

Fig. 3 Comparison of the results of the simplified and refined models: **a** accelerations; **b** displacements

elements, allowed for the identification of the isolated deck dynamic behaviour of the simply supported spans. Comparisons between the frequencies of the frame and refined deck models indicate less than 10% difference between the dominating vertical bending modes, with the higher stiffness of the refined model resulting in slightly higher frequencies at 8.4 Hz and 22.7 Hz for the first two bending modes, respectively. In parallel, the global model, utilising simplified structural elements, was employed to determine mainly the dominant global modes in the lateral direction of the entire bridge structure. The results are presented in Fig. 4 for the deck without consideration of the added track mass and the global structure modelled along with the track, where the first three global lateral modes are presented along with the first two vertical modes of vibration of the deck.

3.2 Track

The track was modelled along with the structure using frame elements connected by springs and dampers representing the rail pads and ballast stiffness. The mass of all non-structural elements was calculated and considered as concentrated masses on the track nodes to represent the

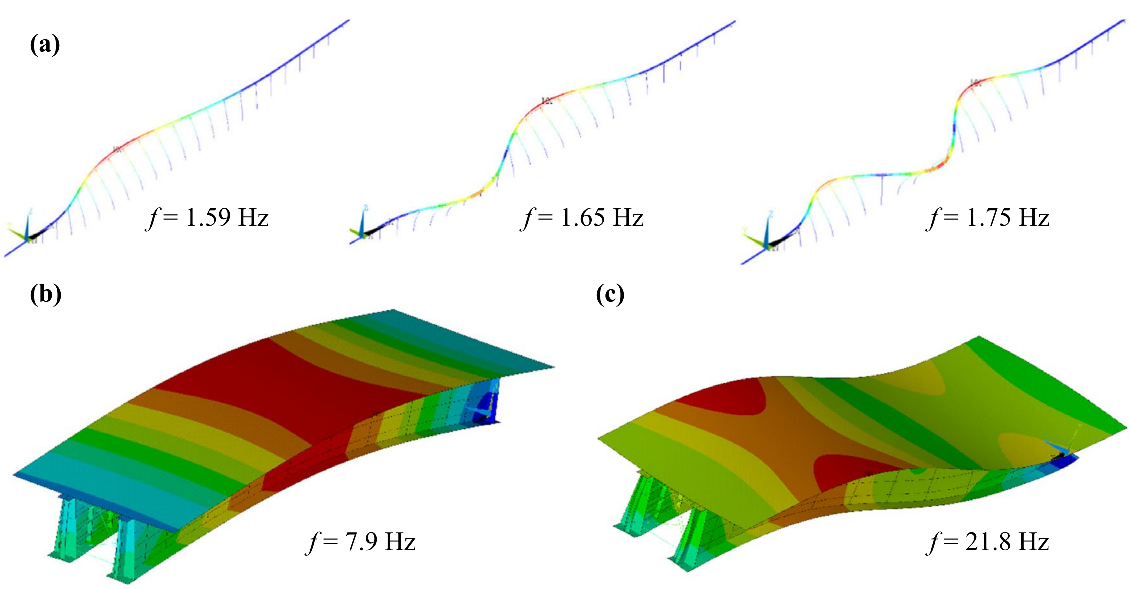

Fig. 4 Modal results of the global (simplified) and deck (refined) models: **a** global bending modes; **b** deck's first vertical bending mode; **c** deck's second vertical bending mode

dynamic behaviour of the track-bridge system accurately. The properties of the springs and dampers used were chosen according to data obtained in Zhai et al.'s work [43], while the rail follows the TR-68 type properties and geometric profile. All track properties considered are given in Table 3. The combined structure-track model using the described methodology is given in Fig. 5. A track section supported by subgrade was modelled before and after the bridge in order to position the vehicle outside of the structure before starting the dynamic analysis in order to establish a realistic dynamic vibration of the vehicle. The vehicle is positioned at least 10 metres before the structure, with its whole length supported by tracks at the beginning of the analysis.

Track irregularities were simulated using the spectrum proposed by the Federal Railroad Administration (FRA), which is commonly adopted in the analysis of the stability of freight trains at lower speeds. The spectrum can be described by power spectral density functions given in Eqs. (7) and (8) for the alignment and elevation spectra, respectively, where coefficients Ω_2 and Ω_3 have the values of 0.1464 rad/m and 0.8168 rad/m, while the A coefficient has values according to the track quality. A six-level classification for track quality can be achieved by adjusting the value of the A according to the values given in Table 4.

$$S(\Omega) = \frac{10^{-7}A\Omega_2^2(\Omega^2 + \Omega_1^2)}{\Omega^4(\Omega^2 + \Omega_2^2)} \quad , \tag{7}$$

$$S(\Omega) = \frac{10^{-7}A\Omega_2^2}{(\Omega^2 + \Omega_1^2)(\Omega^2 + \Omega_2^2)} \quad . \tag{8}$$

The process of generation of track irregularities according to the track spectra proposed by codes can be done using the modified spectral representation method presented by Hi and Schiehlen [44], where the irregularity profile function $r(x)$ is given by the summation of cosine functions of N discrete spatial frequencies Ω_n defined in a frequency interval $[\Omega_0, \Omega_f]$ with increments of $\Delta\Omega$ and random phase angles ϕ_n that are uniformly distributed in the range $[0, 2\pi]$, pondered by amplitudes A_n according to Eq. (9).

$$r(x) = \sqrt{2}\sum_{n=0}^{N-1} A_n \cos(\Omega_n + \phi_n). \tag{9}$$

The final rail deviations for left (l) and right (r) rails in the lateral (y) and vertical (z) directions to be used in numerical simulations can be derived using the relations given in Eq. (10), calculated from the profiles generated for the alignment (A), elevation (V), gauge (G) and cross-level (C) irregularities described previously. Representative values for the peak values and standard deviations expected in both the vertical and lateral irregularities according to the track classes are given in Table 5.

$$\begin{aligned} r_y^{\mathrm{l}}(x) &= r_{\mathrm{A}}(x) + 0.5r_{\mathrm{G}}(x), \\ r_y^{\mathrm{r}}(x) &= r_{\mathrm{A}}(x) - 0.5r_{\mathrm{G}}(x), \\ r_z^{\mathrm{l}}(x) &= r_{\mathrm{V}}(x) + 0.5r_{\mathrm{C}}(x), \\ r_z^{\mathrm{r}}(x) &= r_{\mathrm{V}}(x) - 0.5r_{\mathrm{C}}(x), \end{aligned} \tag{10}$$

The minimum and maximum wavelengths considered were 3 and 25 m, respectively, and sample points were generated at every ten centimetres. A sample of the irregularities considered for levels 3 and 6 proposed by the FRA is given in Fig. 6 as a visual reference for the amplitudes found in different levels of track quality, along with the verification of the spectral properties of the analytical formulation and the artificial profile generated. It is important to note that despite being a stochastic process, only a single

Table 3 Properties of the track

Element	Notation	Parameter	Value
Rail	E	Elasticity modulus	210 GPa
	ρ	Density	7800 kg/m^3
	I_0	Inertia	3.217×10^{-5} m^4
Rail pads	K_{pv}	Vertical stiffness	500×10^6 N/m
	K_{ph}	Horizontal stiffness	20×10^6 N/m
	K_{pl}	Longitudinal stiffness	20×10^6 N/m
	$K_{\mathrm{p}\theta x}$	Longitudinal rotation stiffness	45×10^3 N·m/rad
	$K_{\mathrm{p}\theta y}$	Transversal rotation stiffness	45×10^3 N·m/rad
	$K_{\mathrm{p}\theta z}$	Vertical rotation stiffness	45×10^3 N·m/rad
Ballast	ρ_0	Density	1800 kg/m^3
	K_{bh}	Vertical stiffness	30×10^6 N/m
	K_{bl}	Horizontal stiffness	900×10^3 N/m
	K_{bh}	Longitudinal stiffness	2250×10^3 N/m

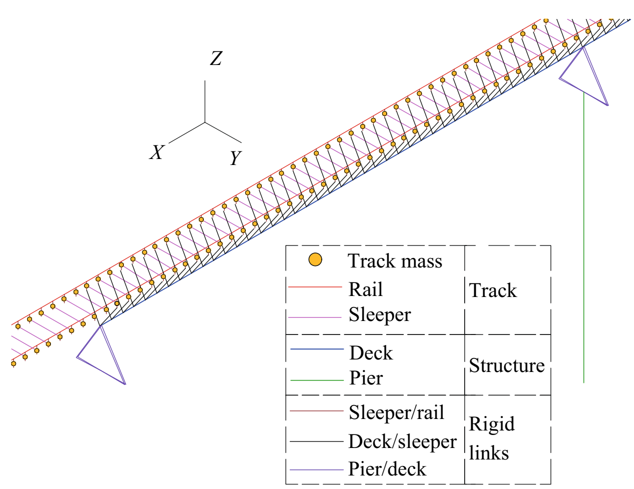

Fig. 5 Structure–track simplified model

representative irregularity profile realization for each level of track quality was considered in this study due to the deterministic nature of the analysis. It is expected, however, that due to the long length of the track, extreme responses are likely to be observed during the crossing.

3.3 Vehicle

Vehicle models used in running safety analyses are most commonly developed using multibody methodology, where concentrated masses are connected by rigid frame elements and adequately chosen springs and dampers. Vehicle properties for multibody models are notoriously difficult to obtain due to industry practices and difficulties associated with performing experimental analyses, resulting in authors choosing to adopt values based on data from the literature. Furthermore, particularities in the development of the finite element or multibody models and simplifications associated with numerical modelling in traditional commercial software can significantly affect the overall dynamic behaviour of the numerical model.

In this paper, we present a strategy based on the use of an optimisation algorithm to fine-tune the properties of the suspensions and mass inertias using the modal characteristics of vehicles obtained in the literature. In this way, it is assured that the dynamic behaviour from the model is well-represented in the vehicle–structure interaction analysis regardless of the modelling strategy used for the vehicle. Two types of vehicles were modelled to represent a typical heavy-haul vehicle composition, namely the locomotive and the gondola-type wagon. Since the analysis is focused on the running safety of the wagons, special focus is given to these vehicles, while the locomotives are used mostly to correctly induce the dynamic effects of their presence in front of the composition. A view of the gondola-type vehicle and its multibody model is given in Fig. 7.

Vehicle mechanical and modal properties were adopted based on data from literature for the locomotives, found in

Table 4 Values of the A coefficient according to the FRA

Class	1	2	3	4	5	6
Max. speed (km/h)	16	40	64	97	129	177
A (m^3/rad)	660.079	376.229	208.841	116.856	65.929	37.505

Table 5 Peak values and standard deviation from vertical and lateral rail irregularity profiles

Class	1	2	3	4	5	6
Peak value (mm)	14.46	13.15	9.05	7.20	5.00	4.12
Standard deviation (mm)	4.76	3.63	2.61	1.99	1.49	1.11

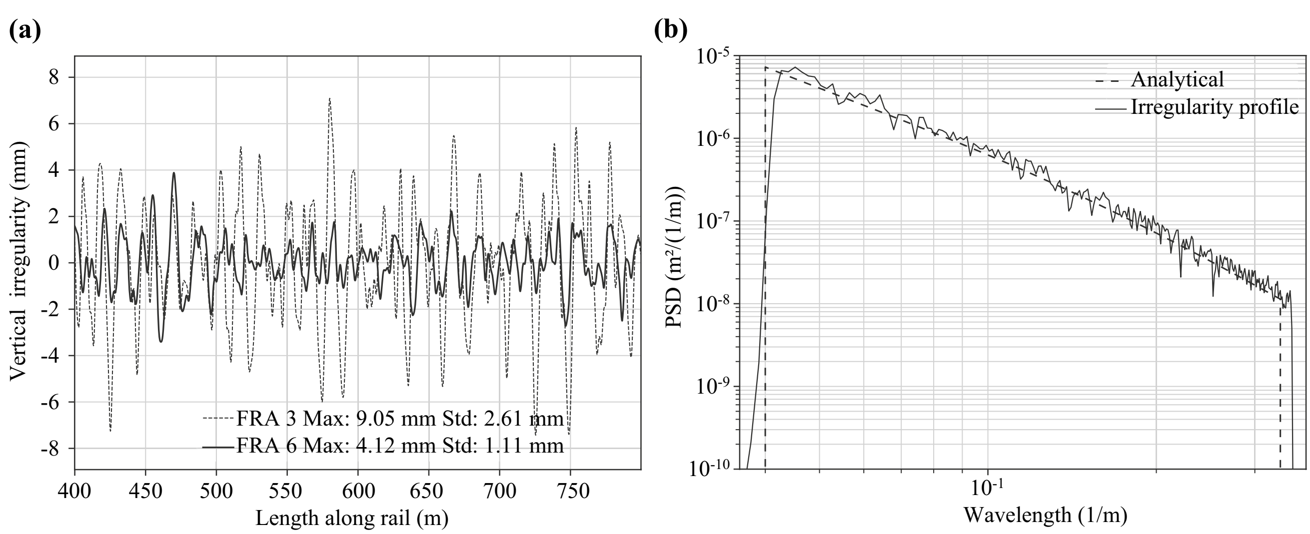

Fig. 6 Track irregularities example: **a** track profile comparison; **b** PSD comparison

Springer

the work of Spiryagin et al. [45], and the loaded ore wagons, as given by Lima et al. [46]. The properties of the unloaded ore wagon, however, were not found in the literature to the best of the authors' knowledge and were adapted based on the tare weight of the wagons and with adjustments to the mass inertias and secondary suspension stiffness parameters that are dependent on carbody weight. The wheel profile follows a standard 1:20 AAR profile as described in similar applications in Brazil [47].

A genetic algorithm was employed to optimise the suspension parameters and mass inertias of the vehicle multibody model, considering slight variations around reference values derived from the literature. The optimisation process aimed to enhance the modal properties, specifically bounce, pitch, yaw, and roll, by minimising the discrepancy between numerical and experimental modal frequencies. To ensure accurate mode identification during the modal analysis, the modal assurance criterion (MAC) was implemented within the algorithm, automatically associating each computed mode shape with its corresponding reference mode based on similarity in eigenvector patterns. By iteratively adjusting stiffness and inertia properties within predefined bounds, the optimisation algorithm fine-tuned the model parameters to achieve maximum alignment with experimentally observed vibration modes described in the literature. This systematic approach improved the model's dynamic fidelity and adjusted the suspension properties from the literature to the specific modelling strategy used in this work. With this, the optimised properties for the vehicles are given in Table 6.

The main focus of the safety assessment in this paper is on the wagons, which display a more unstable dynamic behaviour and tend to present the most critical safety conditions. The most critical element that dictates the dynamic behaviour of this vehicle is the three-piece bogie, composed by the side frames and bolster. The primary and secondary suspensions described in Table 6 are related to the shear pads, and the secondary suspension values are the spring packs, respectively. More detailed information regarding the three-piece bogie is given by Lima et al. [46].

It is important to note that, despite the typical nonlinearities associated with three-piece bogies and heavy-haul vehicles such as friction elements, gaps and clearances, a linearised modelling strategy with spring-damper systems was adopted due to efficiency constraints. Equivalent stiffness and viscous damping coefficients of the shear pads were derived based on hysteresis curves using an approach similar to that of Bragança et al. [48] in order to adequately represent the energy dissipation and stiffness characteristics.

4 Results

In this paper, analyses were performed to study the effects of different degrees of track irregularities according to the profiles presented in Sect. 3.2 using the framework presented in Sects. 2.1 and 2.2 for the vehicle–structure interaction and wheel-rail contact modelling methodologies, respectively. Both loaded and unloaded gondola-type wagons were studied using the models described in Sect. 3.3. The full vehicle composition consisted of two locomotives followed by five wagons due to computational constraints and was chosen since it was able to accurately represent the dynamic responses of both systems due to the simply supported nature of the bridge structure.

Analyses were performed for the speed ranges between 40 and 120 km/h, at 10 km/h increments, for the track irregularities classes of 3 (worst conditions) to 6 (best conditions). The results were investigated both in terms of structural and

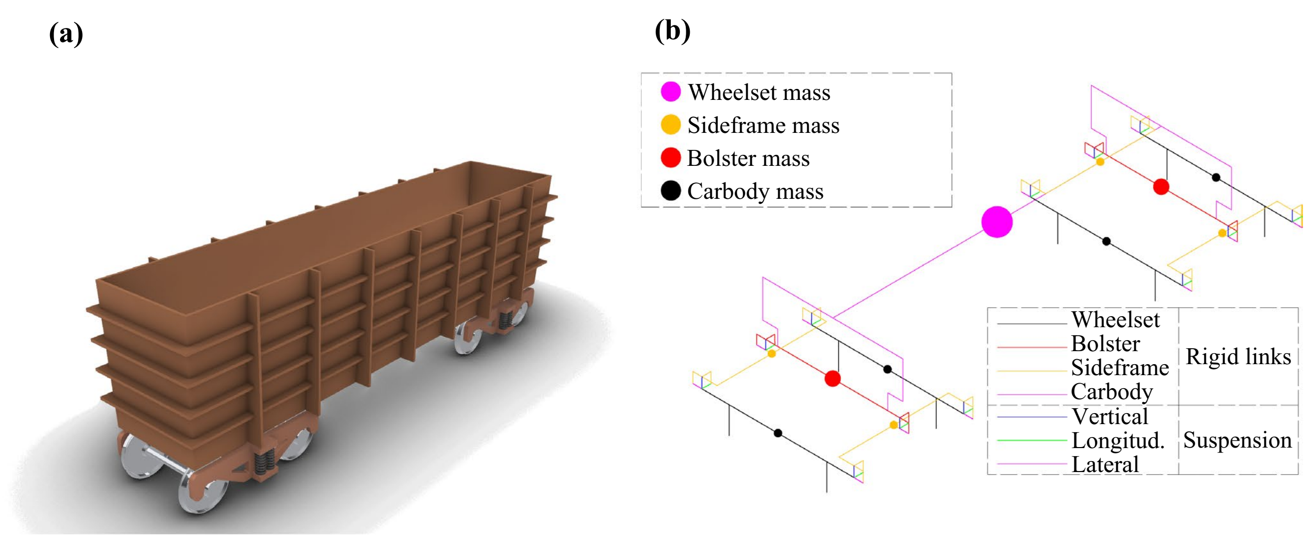

Fig. 7 Heavy-haul ore wagon: **a** general view; **b** multibody model

Table 6 Properties of the vehicles

Element	Symbol	Parameter	Locomotive	Loaded wheelset	Unloaded wheelset	Unit
Carbody	m_c	Mass	91, 600	138, 000	25, 000	kg
	I_{cy}	Pitch inertia	177×10^3	180.0×10^3	75.0×10^3	kg·m^2
	I_{cx}	Roll inertia	3.77×10^6	0.94×10^6	15.0×10^3	kg·m^2
	I_{cz}	Yaw inertia	3.97×10^3	0.99×10^6	80.0×10^3	kg·m^2
Bogie	m_b	Mass	11, 000	3, 500	3, 500	kg
	I_{by}	Pitch inertia	2.70×10^3	1.50×10^3	1.50×10^3	kg·m^2
	I_{bx}	Roll inertia	2.83×10^3	1.20×10^3	1.20×10^3	kg·m^2
	I_{bz}	Yaw inertia	4.23×10^3	1.35×10^3	1.35×10^3	kg·m^2
Wheelset	m_w	Mass	3,400	1,800	1,800	kg
	I_{wx}	Roll inertia	2.00×10^3	1.5×10^3	1.5×10^3	kg·m^2
	I_{wz}	Yaw inertia	3.50×10^3	1.5×10^3	1.5×10^3	kg·m^2
Primary suspension	K_{1x}	Long. stiffness	1.44×10^6	2.15×10^7	2.15×10^7	N/m
	K_{1y}	Lat. stiffness	5.70×10^6	5.59×10^7	5.59×10^7	N/m
	K_{1z}	Vert. stiffness	2.10×10^6	2.34×10^7	2.34×10^6	N/m
	C_{1x}	Long. damping	9.00×10^3	9.00×10^3	9.00×10^3	N·s/m
	C_{1y}	Lat. damping	27.90×10^3	25.00×10^3	25.00×10^3	N.s/m
	C_{1z}	Vert. damping	25.00×10^3	10.00×10^3	10.00×10^3	N·s/m
Secondary suspension	K_{2x}	Long. stiffness	0.33×10^6	2.22×10^7	2.22×10^7	N/m
	K_{2y}	Lat. stiffness	0.33×10^6	3.82×10^6	3.82×10^7	N/m
	K_{2z}	Vert. stiffness	1.07×10^6	6.73×10^6	4.73×10^6	N/m
	C_{2x}	Long. damping	30.00×10^3	30.00×10^3	30.00×10^3	N·s/m
	C_{2y}	Lat. damping	79.00×10^3	45.00×10^3	45.00×10^3	N·s/m
	C_{2z}	Vert. damping	45.00×10^3	150.00×10^3	150.00×10^3	N·s/m

vehicle responses, with special focus on train running safety indices as described in Sect. 2.3, focusing on the unloading and Nadal coefficients.

4.1 Comparison with moving load models

With the fully developed structure models, the first analysis performed consisted of comparing the dynamic responses of the bridges while using the conventional moving loads model and the vehicle–structure interaction methodology to verify the accurate representation of structural dynamic behaviour. Results for midspan accelerations and displacements are presented in Fig. 8 for one case of the loaded vehicle running at 120 km/h, showing good agreement between both methods. Notably, the solution using the vehicle–structure interaction method leads to high-frequency vibrations in the structure due to the consideration of track irregularities. Slightly increased displacements during the crossing of the wagons are also observed, which can be explained by the frequent wheel impacts caused by the influence of track irregularities and are particularly more significant for the loaded wagon due to its dynamic characteristics and significantly increases its dynamic load.

4.2 Comparative analyses

To investigate the influence of track quality on the dynamic response of the systems, the results of a comparative analysis at a constant vehicle speed of 80 km/h are presented in this section, considering the different classes of track irregularities. For each irregularity class, time histories of displacements, accelerations, contact forces and derailment indexes are calculated and presented. With this, a visual comparison is provided to highlight qualitative differences in system behaviour as a function of track condition.

4.2.1 Dynamic response comparisons

In this section, time histories of displacements and accelerations were extracted for the midspan node of one of the spans of the bridge and one of the vehicle's carbody and a comparison is presented for different degrees of track irregularity. This qualitative comparison is provided in Fig. 9 and

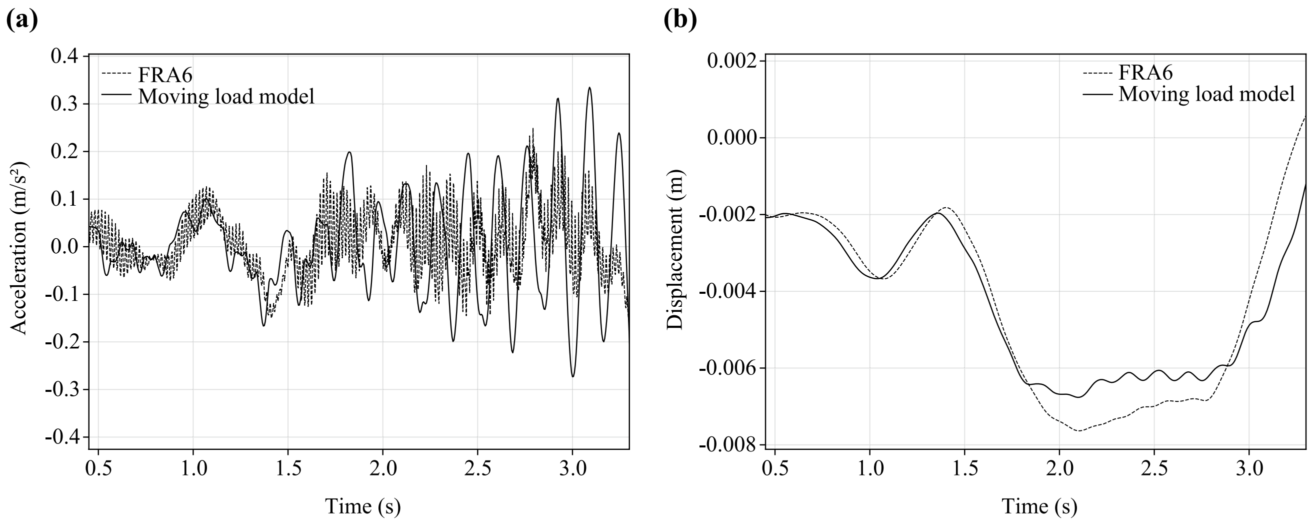

Fig. 8 Comparison of the results of the moving load and interaction methods: **a** accelerations; **b** displacements

can be used to visualise the effects of track quality on the dynamic responses of the structure and vehicle.

The results in Fig. 9b show that the bridge displacements exhibit minimal sensitivity to the level of track irregularity, with only minor variations observed across the different scenarios. In contrast, deck accelerations described in Fig. 9a show a noticeable increase in magnitude as the severity of the irregularities increases. Regarding the vehicles, vertical accelerations shown in Fig. 9c remain relatively consistent across all cases, with slightly higher peaks for higher degrees of irregularity. However, lateral accelerations given in Fig. 9d are significantly more pronounced under poorer track conditions, indicating a stronger dynamic interaction in the lateral direction and emphasising the importance of track quality for vehicle safety.

4.2.2 Running safety comparison

To assess the impact of track irregularities on train running safety, time histories of the Nadal and the wheel unloading coefficients were computed at each time step, providing a view of the safety of the vehicle while crossing the bridge and plotted in Fig. 10.

As expected from the more pronounced lateral vehicle responses observed under rougher track conditions, the Nadal coefficients given in Figs. 10a and b for the locomotives and wagons, respectively, increase with the severity of the irregularities. Notably, lateral contact forces and consequently the Nadal coefficients are consistently higher throughout the whole crossing due to the worse track conditions, which demonstrate the effects of track irregularities on the lateral behaviour of the vehicle. Furthermore, the Nadal coefficient behaviour does not present significant differences between the locomotive and wagon wheels.

On the other hand, the unloading coefficient given in Figs. 10c and d shows a less consistent response. While its baseline levels are only slightly elevated for the rougher tracks, peaks are observed more frequently and severely in tracks with higher degrees of irregularity. These isolated events indicate localised reduction of the vertical contact force associated with higher values of the vertical track irregularities in specific points on the track, which occur more frequently in degraded conditions. For smoother tracks, unloading remains consistently low, suggesting that vertical safety margins are largely preserved even under non-negligible irregularities. Comparison between the locomotive and wagons shows that the high-stiffness suspensions of the latter lead to more severe vertical oscillations and higher variation of vertical contact forces, which demonstrates the high variations of dynamic loads, more frequent impacts on the track and loss-of-contact situations, which may affect their running safety.

Irrespective of the track quality, it is clearly observed that both in the case of vehicle accelerations and running safety indices, pronounced oscillations of the vehicle occur during the crossing of the bridge, indicating a less stable riding condition. This behaviour is strongly influenced by the vehicle type, particularly the suspension configuration and stiffness. Freight vehicles, which are equipped with a single-stage suspension system characterised by relatively high stiffness, exhibit higher vertical and lateral accelerations compared

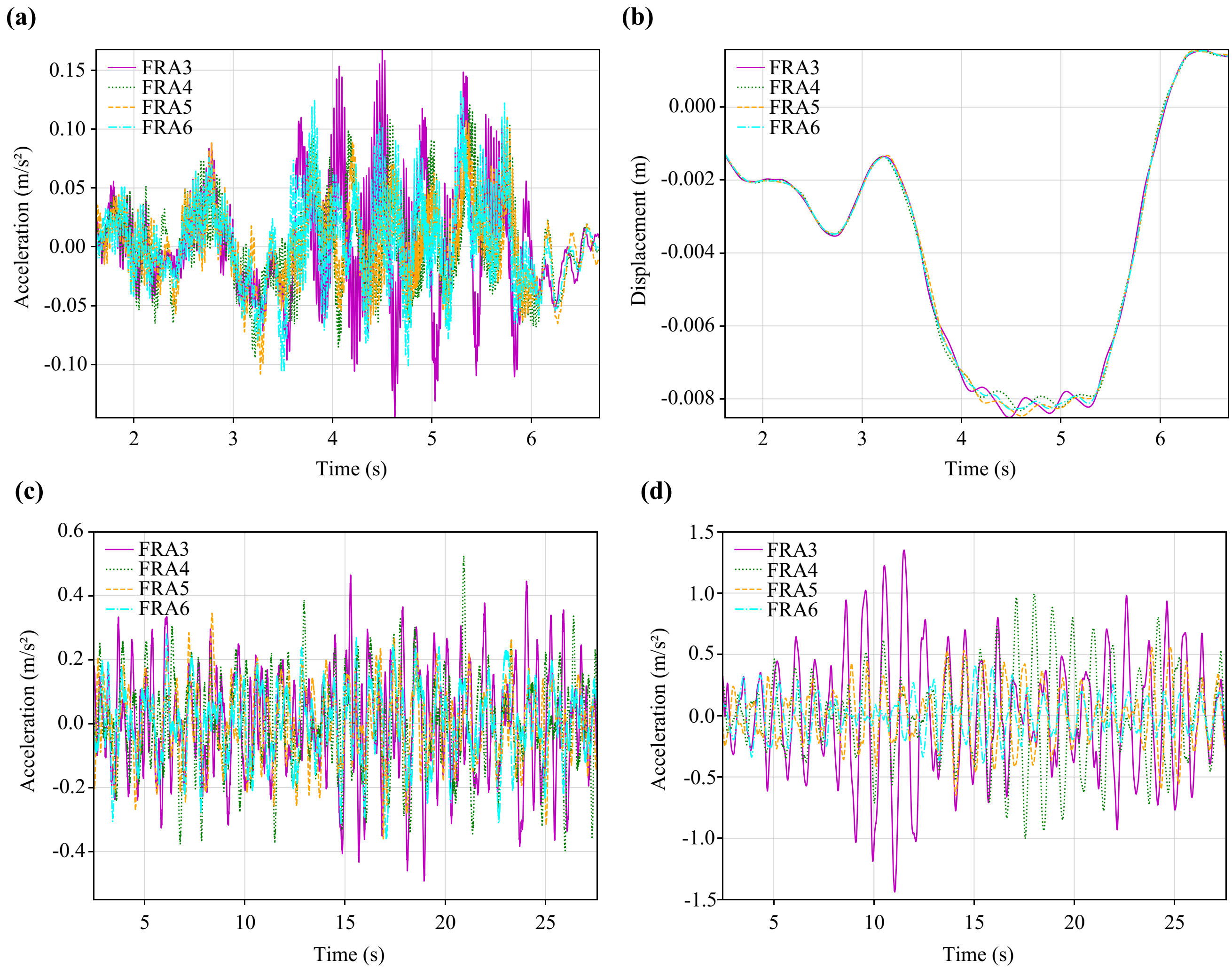

Fig. 9 Comparison of the dynamic responses at 80 km/h: **a** bridge vertical accelerations; **b** bridge vertical displacements; **c** vehicle vertical accelerations; **d** vehicle lateral accelerations

to passenger coaches or locomotives, which are designed to absorb and damp undesired vibrations. In contrast, vehicles with more advanced suspension layouts, such as multi-stage systems in high-speed or locomotives themselves, demonstrate improved dynamic performance and enhanced safety margins under the same track conditions. The locomotives, while subjected to significant forces due to their mass, benefit from more robust suspension designs, which help limit the severity of dynamic effects observed in the trailing freight wagons.

4.3 Systematic analyses

In this section, a systematic evaluation of the peak dynamic responses observed during the simulations is presented, with the objective of assessing both the structural safety of the bridge and the running safety of the train. For the bridge, the analysis considers the maximum vertical and lateral displacements and accelerations, identified across all spans and over the whole duration of the crossing. For the vehicles, attention is focused on the freight wagons, for which the highest vertical and lateral accelerations at the carbody level were recorded, as well as the maximum values of the Nadal and unloading coefficients computed across all wheels. These envelope values allow for a comprehensive comparison of the dynamic effects induced by different levels of track irregularity and characterisation of the safety of all subsystems. The results are presented for both loaded and unloaded train configurations, enabling the quantification and discussion of how loading conditions influence the system's dynamic behaviour and safety margins.

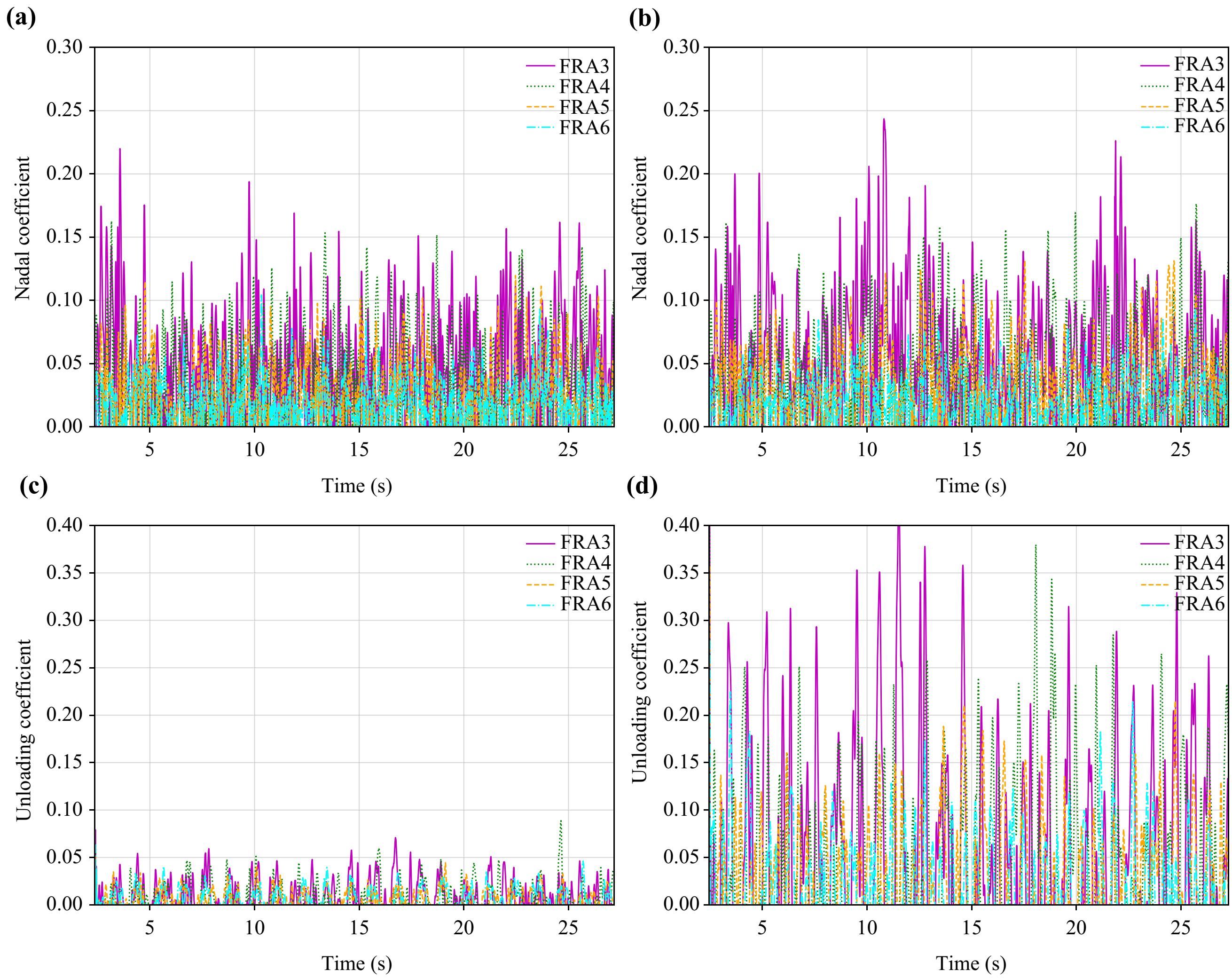

Fig. 10 Comparison of the running safety at 80 km/h: **a** Nadal coefficient of the locomotive; **b** Nadal coefficient of the wagon; **c** unloading coefficient of the locomotive; **d** unloading coefficient of the wagon

4.3.1 Loaded vehicle

At first, the maximum dynamic responses obtained for the bridge and the vehicle carbodies are presented in Fig. 11, which provides insights into the structural responses and overall vehicle behaviour. For the bridge, the results include the peak vertical and lateral displacements and accelerations, while for freight wagons, the maximum vertical and lateral accelerations observed at the carbody level are given. These quantities reflect the combined influence of track irregularities and vehicle–structure interaction under full loading conditions.

Considering the bridge responses obtained, a distinct contrast between the vertical and lateral directions can be observed. While vertical displacements remain remarkably consistent across all track irregularity levels with small absolute variations in their maximum values, consistent with what was observed in Fig. 9b, lateral displacements exhibit a clear increase as the track condition deteriorates. A similar trend is observed in the acceleration responses, where both vertical and lateral accelerations increase with higher degrees of irregularity, with particularly noticeable amplification for track class 3. Regarding the influence of vehicle speed, lateral responses show limited sensitivity, whereas vertical accelerations do increase with higher vehicle speeds. Importantly, all displacement and acceleration values remain well below any structural safety thresholds, which are not displayed in the graphs for clarity, indicating that the bridge maintains adequate performance and integrity under all investigated conditions.

Regarding vehicle responses, the vertical accelerations of the wagon carbodies exhibit a clear and consistent dependence on both track irregularity and vehicle speed. As the severity of the irregularities increases, or as the train

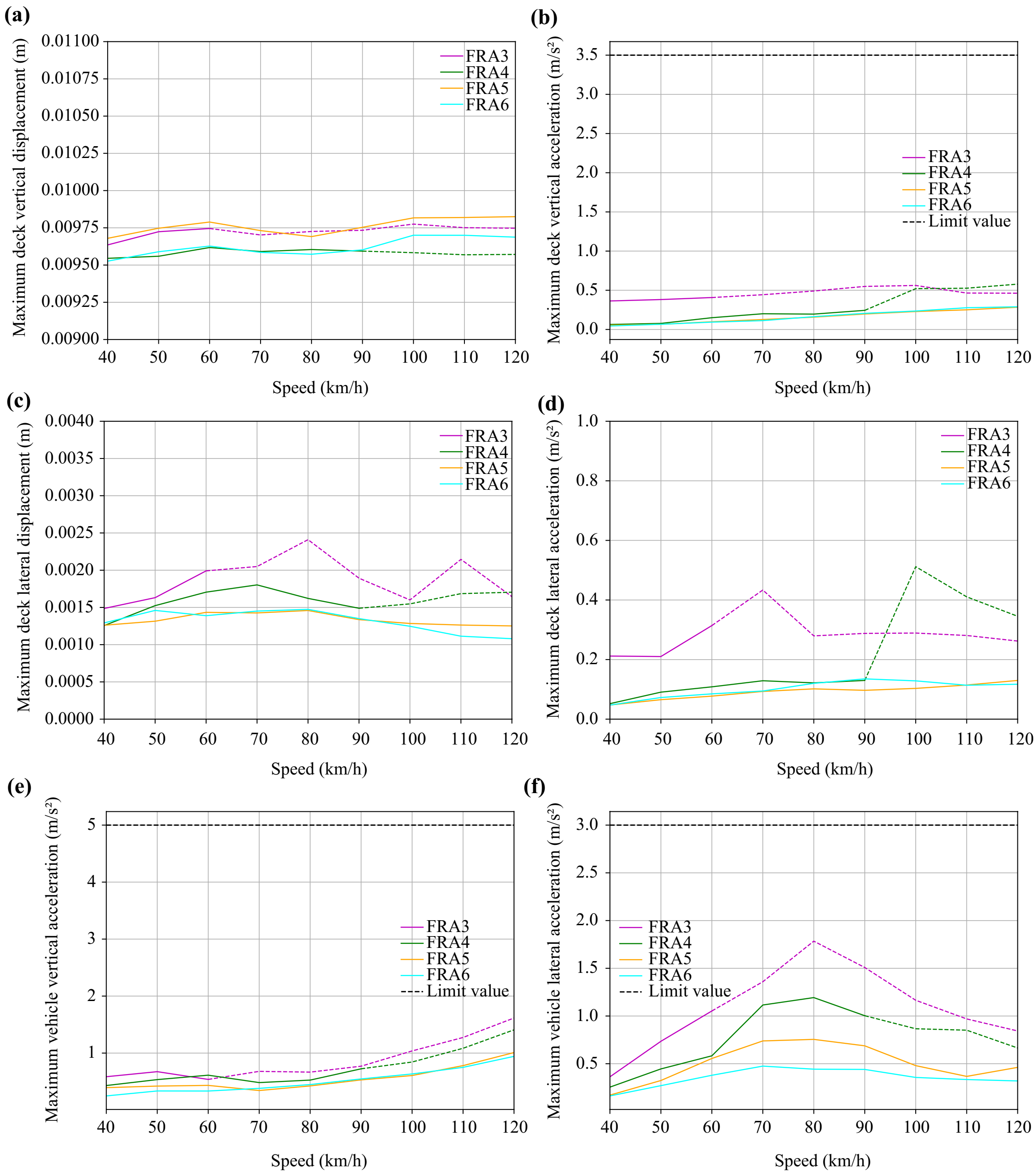

Fig. 11 Maximum bridge and vehicle responses for the loaded vehicle: **a** bridge vertical displacements; **b** bridge vertical accelerations; **c** bridge lateral displacements; **d** bridge lateral accelerations; **e** vehicle vertical accelerations; **f** vehicle lateral accelerations

travels at higher speeds, the vertical dynamic responses grow noticeably, indicating strong coupling between excitation input and vertical vehicle dynamics, as expected. In the lateral direction, the accelerations also increase with worsening track quality. Considering the different train speeds, lateral accelerations reach a pronounced peak at 80 km/h, which is attributed to a speed-dependent excitation mechanism associated with the periodic variation of vertical support stiffness as the vehicle traverses the sequence of simply supported spans. At this speed, the corresponding span-passing frequency approaches the wagon's carbody roll frequency, enabling a coherent and cumulative excitation over multiple spans. Although the stiffness modulation is vertical in nature and does not directly excite a pure roll resonance, its interaction with track irregularities and wheel–rail contact dynamics leads to amplified lateral vehicle response. It should be noted that all responses are within normal parameters and that the high peaks observed for the lateral responses are well outside the recommended speeds for Class 3 track conditions as shown in Table 4, demonstrating the need to establish proper track conditions for traffic and validating the recommendations for track irregularities defined by the Federal Railroad Administration.

The results of the running safety indices given in Fig. 12 further reinforce the trends observed in the dynamic response analysis. The Nadal coefficient increases consistently with higher degrees of track irregularity, reflecting the more severe lateral excitation experienced by the wheels. However, even under the most degraded track conditions, the values remain comfortably below the established safety threshold. However, despite the inherently large static axle loads of freight wagons, significantly elevated unloading coefficient values are observed, especially for the worst track classes. These results underscore the behaviour of heavy-haul freight wagons' single-stage suspension systems with high stiffness, which leads to pronounced vertical oscillations and limited vibration isolation. Nevertheless, all safety indicators remain within acceptable limits, even at speeds beyond the recommended operational range for each track class, indicating that the vehicle–track system maintains safe performance throughout the scenarios analysed for the loaded vehicle.

4.3.2 Unloaded vehicle

The analysis of the unloaded vehicle is also essential to characterise the dynamic behaviour of freight wagons under tare loading conditions, which can occur in return trips when no cargo is being transported back. In this case, the vehicles operate with substantially reduced mass, and although the suspensions are designed to work with lower stiffnesses, the system remains characterised by a relatively stiff single-stage suspension. As a result, the suspension's limited capacity for vibration isolation becomes more pronounced, leading to dynamic characteristics that are inherently more sensitive to irregularities and dynamic amplification, particularly in the vertical direction. Overall, the traffic conditions for the unloaded wagons can be considered more unstable than those of the loaded case, and their running stability requires careful assessment under realistic operational scenarios.

The results are compiled in Fig. 13. Considering the bridge responses obtained for the unloaded configuration, the vertical behaviour follows a similar trend to that observed in the loaded case. Similarly, vertical displacements remain consistent across all irregularity classes with small absolute variations, but with notably lower magnitudes than in the loaded case due to the reduced mass of the vehicles. For vertical accelerations, the overall pattern remains similar, but in the unloaded configuration, higher peak values can be observed in some cases, indicating that the more unstable vertical behaviour of the vehicle contributes to increased excitation of the bridge. In the lateral direction, both displacements and accelerations show very similar values and overall behaviour when compared to the loaded case, with no significant amplification attributable to the vehicle mass. These results confirm that the bridge response remains well within safe limits under tare loading and that the structural performance is not adversely affected by the transition from loaded to unloaded operation, although

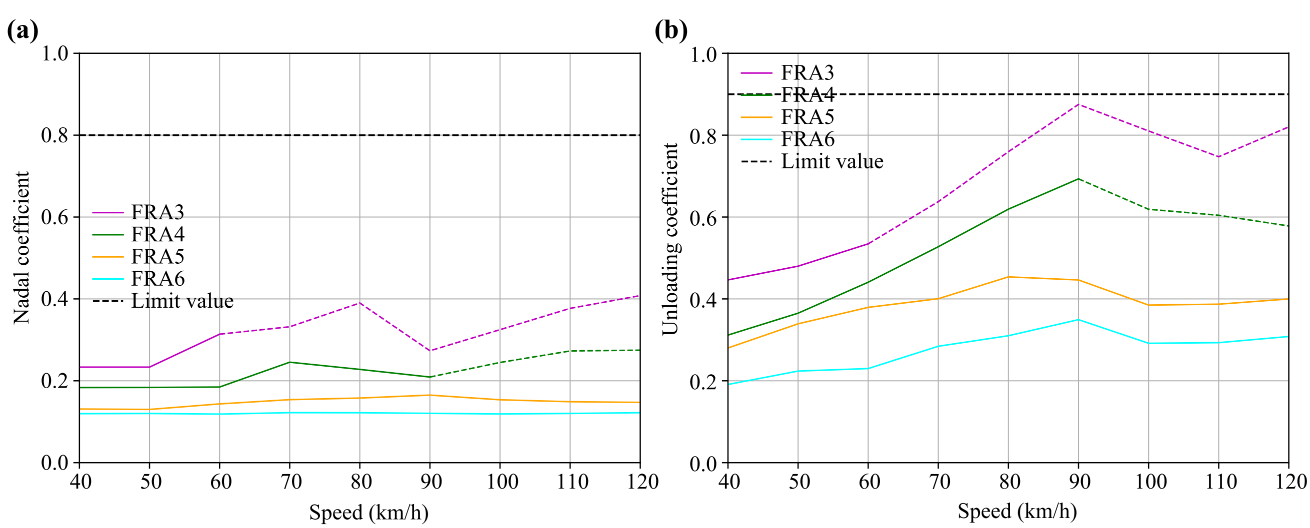

Fig. 12 Maximum running safety coefficients for the loaded vehicle: **a** Nadal; **b** unloading

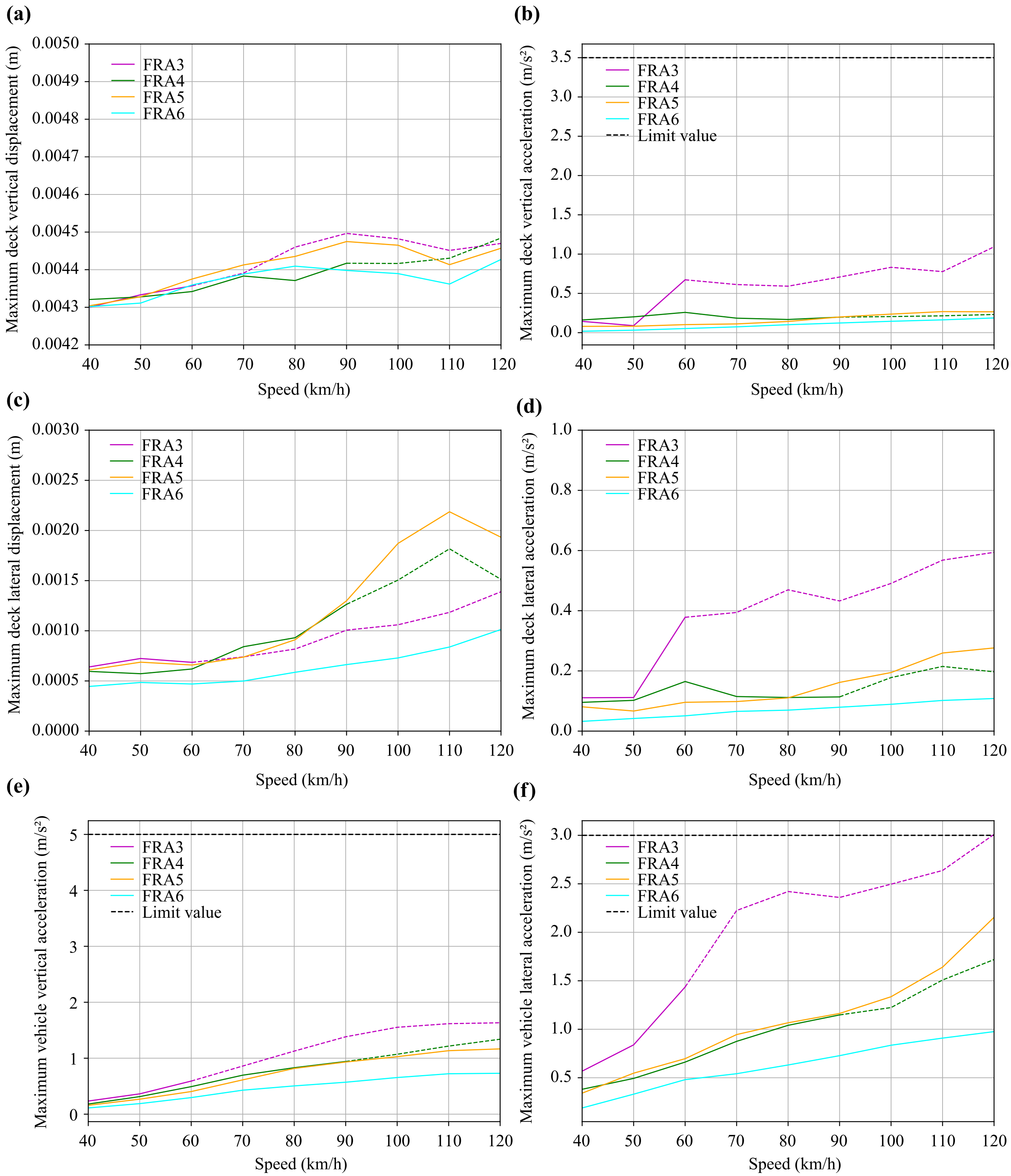

Fig. 13 Maximum bridge and vehicle responses for the unloaded vehicle: **a** bridge vertical displacements; **b** bridge vertical accelerations; **c** bridge lateral displacements; **d** bridge lateral accelerations; **e** vehicle vertical accelerations; **f** vehicle lateral accelerations

some results can be affected by the more unstable vehicle behaviour.

The vehicle responses in the unloaded configuration exhibit the same general trends observed in the loaded case, with dynamic responses increasing both with higher degrees of track irregularity and with vehicle speed. However, the magnitudes of the responses are distinctly different, especially for the lateral accelerations, which are significantly higher across all conditions when compared to the loaded case, while vertical accelerations are only slightly elevated at higher speeds. These differences highlight the greater sensitivity of the unloaded wagons to dynamic excitation, stemming from their reduced mass and the stiff suspension system. Although the qualitative behaviour remains consistent, the increase in acceleration levels clearly reflects more unfavourable traffic conditions and reduced dynamic stability in the unloaded configuration.

The impact of the unstable vehicle dynamic behaviour in the unloaded conditions becomes more evident when evaluating the running safety indices, which are presented in Fig. 14. The Nadal coefficients continue to follow the same trends observed for the loaded vehicles, but their values are significantly higher across all scenarios. This indicates a higher ratio of lateral to vertical contact forces, resulting from the reduced vehicle mass and increased lateral vibrations. Despite this amplification, the Nadal coefficients remain within acceptable safety limits. On the other hand, the unloading coefficient shows more critical results with violation of the limit values and loss of contact being observed in nearly all irregularity classes, with the exception of the track class 6. The combination of lower axle loads and higher vertical excitations leads to frequent occurrences of loss of contact across most scenarios, which can seriously threaten running safety.

Due to the violations of the limit values, further exploration of the results of the analysis is provided to establish train running safety using more sophisticated approaches. The aim of this extended investigation is to refine the interpretation of the unloading index by incorporating temporal characteristics of the contact loss events, offering a more realistic assessment of derailment risk, which are presented in Fig. 15. For this, the percentage of time of the crossing during which the unloading criterion is exceeded is studied. Then, the characteristics of the loss-of-contact scenarios are presented, with the number of occurrences, and their maximum and average time. Finally, using the alternative criterion that derailment will occur if the wheel loses contact for a given time duration, the safety of the trains is defined for all studied scenarios.

First, the duration over which the unloading coefficient exceeds the critical threshold throughout each simulation is examined, which allows the quantification of how persistent these safety-critical conditions are. In Fig. 15a, it is clear that for worse track conditions and higher train speeds, the criterion is exceeded much more often, which gives a more nuanced view of the behaviour of the unloading coefficient. Additionally, the frequency of contact loss events for each scenario is given in Fig. 15b, and, for those events, the maximum and average uninterrupted duration in which the wheel remained detached from the rail is calculated and presented in Figs. 15c and d. This approach allows us to demonstrate that, although the index limit is exceeded across all scenarios, more degraded track conditions consistently lead to more frequent contact loss and with longer durations, thus indicating a greater threat to train running safety. It is observable in Figs. 15c and d that the time of contact loss events is higher for low train speeds, demonstrating that the slower vehicle recovers more slowly to loss-of-contact situations and that the high-stiffness suspension system leads

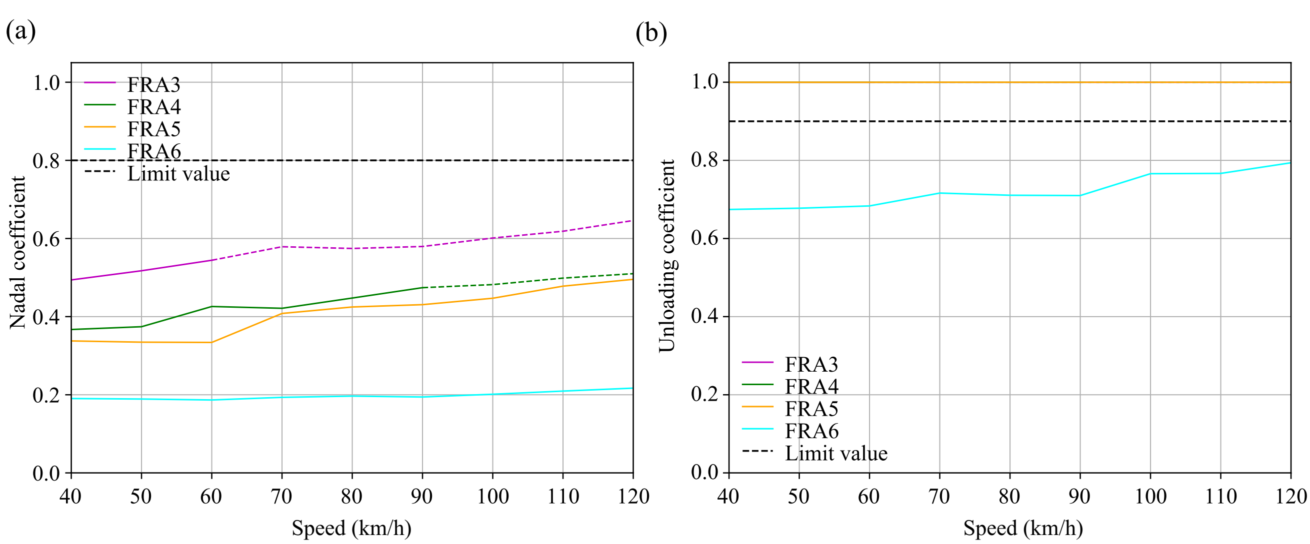

Fig. 14 Maximum running safety coefficients for the unloaded vehicle: **a** Nadal; **b** unloading

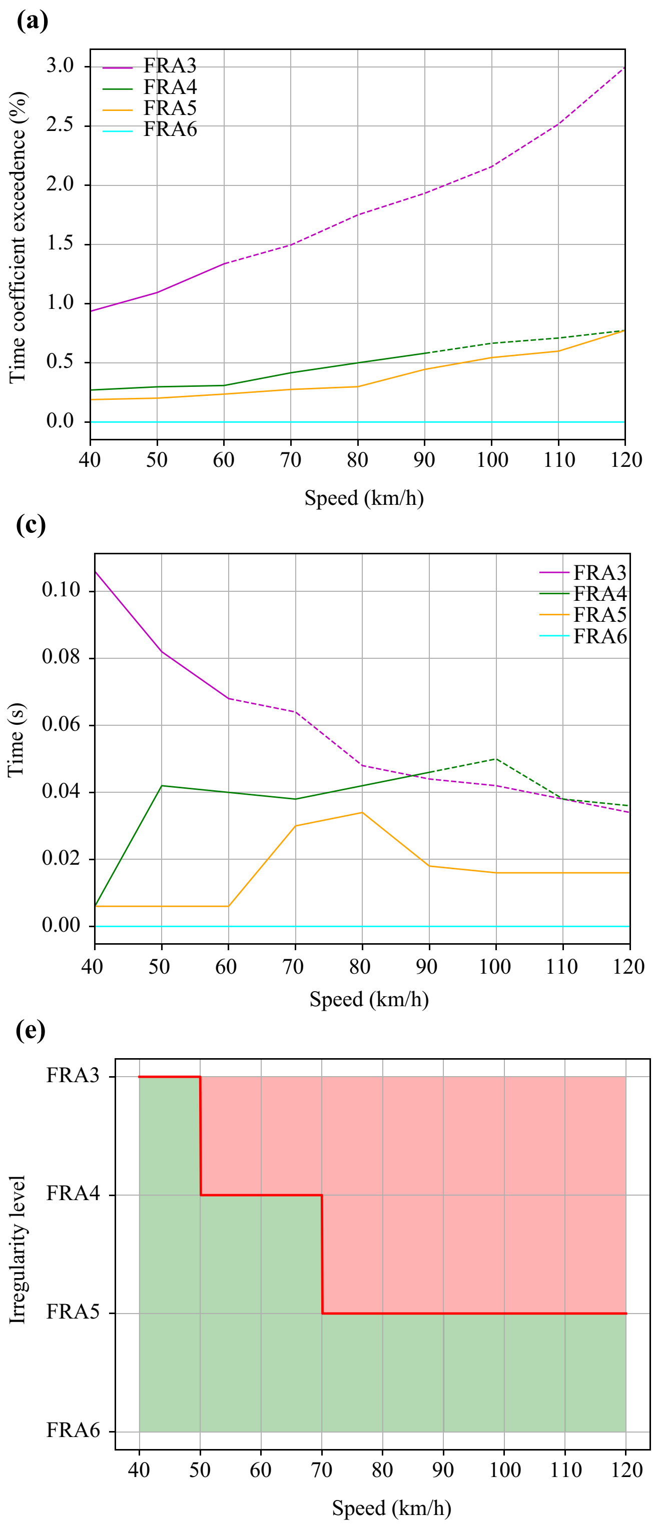

Fig. 15 Temporal analysis of unloading situations: **a** Percentage of time exceeding 0.9; **b** number of loss-of-contact occurrences; **c** maximum time of loss of contact; **d** average time of loss of contact; **e** loss-of-contact safety; **f** unloading coefficient safety

to stronger oscillations, threatening running safety. Furthermore, contact loss duration time reduces with increasing speed, which shows that high-frequency oscillations lead to more frequent loss of contact that can be harmful to running safety and further demonstrates the lack of ability of the high-stiffness suspensions to adapt to the vertical

Springer

track irregularity profiles. Thus, in most scenarios, the poor dynamic capabilities associated with the high-stiffness suspensions and lower mass of the vehicle lead to unsafe traffic conditions due to the lack of capability of the suspensions to isolate the movement of the carbody from the wheels and causing frequent loss of contact, even at lower speeds.

Finally, a more realistic derailment criterion discussed by [8] is employed, where a loss-of-contact duration exceeding 15 ms is considered unsafe. Using this threshold, cases in which safety margins are maintained despite transient violations are identified, enabling a more nuanced evaluation of the vehicle's running safety. This is given in Fig. 15e, where we can establish safe conditions for a wider range of train speeds and track conditions than previously shown in Fig. 14b. This underscores the importance of a realistic investigation into the wheel-rail contact behaviour and reassures that running safety can still be guaranteed for more operational conditions, showing that only the worst track conditions are incompatible with the traffic of the unloaded vehicle.

4.4 Discussion

The results obtained for the bridge were explored for both vertical and lateral dynamic behaviour under varying track conditions and vehicle configurations. Across both loaded and unloaded cases, vertical displacements remained consistently low and relatively insensitive to track irregularities, with even lower magnitudes observed in the unloaded scenario due to the reduced vehicle mass. However, vertical accelerations were more affected by changes in track quality, particularly under degraded conditions, and were notably higher for the unloaded case, indicating the greater dynamic amplification associated with the lighter and more unstable vehicles. In contrast, lateral displacements and accelerations showed more pronounced increases with track degradation but exhibited minimal sensitivity to changes in vehicle speed. Overall, all bridge responses remained safely below structural limits, reaffirming the good structural performance of the bridge under the full range of simulated scenarios, which is owed to the adequate design procedures for such heavy loads, leading to an extremely stiff and resistant structure.

Different dynamic behaviours and the consequences to running safety coefficients for the locomotives and wagons were also briefly shown in Sect. 4.2.2. As discussed, the more sophisticated suspension system of the locomotive leads to a more stable riding condition, which is reflected in the overall running safety. A comprehensive comparison of the maximum running safety coefficients of the different types of vehicles for the best track conditions is presented in Fig. 16. For the Nadal coefficients, the vehicle characteristics hold less importance than the track conditions, and even then, the unloaded vehicle has significantly worse running safety indices due to its smaller mass. For the unloading coefficient, the stiff suspensions lead to more variation of the vertical forces and more unstable riding conditions. Even in the comparison between similar axle loads from the loaded vehicle and locomotive, the beneficial effects of the two-stage suspension of the locomotive are clearly reflected in the significantly smaller unloading coefficient, even at higher speeds.

The wagon dynamic responses demonstrated consistent trends across both configurations, with clear increases in both vertical and lateral accelerations as track quality deteriorated and vehicle speed increased. These effects were amplified in the unloaded scenario, especially in the lateral direction, where significantly higher accelerations were

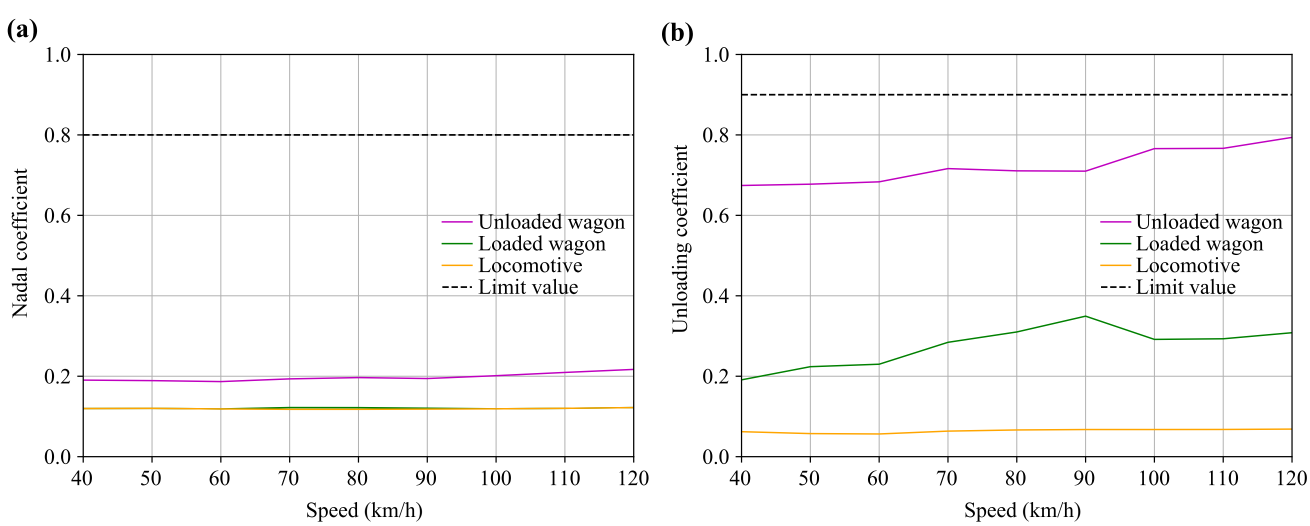

Fig. 16 Comparison of maximum responses for all vehicles: **a** Nadal; **b** unloading

observed. The unloaded wagons exhibited more unstable dynamic behaviour due to their reduced mass and the relatively stiff single-stage suspension system, which limits vibration isolation and leads to higher sensitivity to irregularities. The loaded configuration, although subject to similar influences, displayed more stable responses overall, with dynamic effects better mitigated by the higher mass and consequently inertia, which helps to stabilise the vehicle behaviour. These findings emphasise the importance of considering both loading conditions and track quality when assessing freight wagon dynamics.

Finally, the evaluation of running safety coefficients demonstrated the strong relation between vehicle dynamics and its stability, as well as the role played by the inherently unstable dynamic characteristics of the heavy-haul vehicles. Nadal coefficients increased consistently with track quality degradation and were substantially higher in the unloaded configuration due to the reduced vertical loads and more unstable lateral responses, although they remained below conventional safety thresholds. Furthermore, comparisons between all three vehicle types show that, although vehicle dynamics play a part in running safety, track quality is significantly more relevant for the evaluation of the Nadal coefficient. Unloading coefficients, on the other hand, presented a more severe outcome. While the loaded wagon maintained wheel-rail contact in all scenarios, it is still relevant that under higher degrees of track irregularities, the unloading coefficient is quite significant, which reflects the challenging dynamic behaviour of the high-stiffness single-stage suspension system. Nevertheless, the traffic conditions remain stable and safe for all scenarios investigated due to the high mass and inertia of the loaded carbody. Considering the unloaded vehicle, it was observed that the empty wagons experienced frequent loss of contact under nearly all track conditions except the smallest track irregularities. This reflects the limitations of high-stiffness suspensions in isolating vertical vibrations, both at low speeds, where irregularity-induced disturbances lead to longer durations of contact loss and also for high-frequency oscillations at higher speeds. The subsequent analysis on contact loss duration confirmed that running safety is more severely threatened in tracks with higher degrees of irregularity, but safety could still be argued for a wider range of speeds and conditions than the simplified threshold-based criteria, underscoring the need for refined evaluation approaches that incorporate time-domain safety metrics and sophisticated modelling techniques.

5 Concluding remarks

This study addressed a rarely investigated topic in the literature of bridge engineering concerning the dynamic behaviour and running safety of heavy-haul freight railway vehicles, which are frequently subjected to degraded track conditions and have inherently more unstable dynamic characteristics. To this end, a comprehensive numerical framework was developed, integrating a vehicle–structure interaction model with nonlinear wheel-rail contact modelling, placing particular focus on accurately representing freight wagons. The structure was modelled and calibrated in a finite element modelling environment, and a vehicle multibody modelling strategy was adopted considering linearised suspension elements with mechanical properties calibrated based on the use of optimisation algorithms aiming at correctly representing modal properties of the wagons found in the literature, ensuring realistic dynamic behaviour.

The validated models were employed to perform a wide set of deterministic dynamic simulations encompassing different degrees of track quality considered by employing a representative realisation of track irregularity profiles and a broad range of operational speeds for both the loaded and unloaded vehicle configurations. The analyses confirmed that bridge responses remained within safe limits in all scenarios, while vehicle responses, especially in the unloaded case, highlighted the dynamic amplification effects caused by track irregularities and the inherently challenging dynamic behaviour of the heavy-haul wagons. The running safety assessment further reinforced these findings, showing that while limit-based criteria were occasionally exceeded, more refined time-domain metrics provided a nuanced and realistic picture of train safety.

Overall, the results presented in this work emphasise the importance of realistic modelling and detailed dynamic assessment of bridge crossings for freight operations, especially under challenging track and loading conditions. The framework and findings offer insights for future studies on stability analyses of heavy-haul vehicles and assist infrastructure managers and rolling stock designers in evaluating and improving the safety and performance of heavy-haul transport systems. Furthermore, the results show the need for further investigations into the implementation of adequate running safety criteria for these types of vehicles under varied track and loading conditions. Finally, due to the stochastic nature of the main source of excitation, a proper probabilistic methodology is necessary for a comprehensive safety evaluation of this problem and will be the object of future work.

Acknowledgements The authors would like to acknowledge Matheus Souza and VALE for making available the plans and data for the structure, and Letícia Santana Nery and Dr João Victor Fragoso Dias for their contributions to the modelling of the three-dimensional model.

• This work was financially supported by Base Funding (UIDB/04708/2020) and Programmatic Funding(UIDP/04708/2020) of the CONSTRUCT—Instituto de I&D em Estruturas e Construções—funded by national funds through the FCT/MCTES (PIDDAC).

• Grant No. 2022.00628.CEECIND from the Stimulus of Scientific Employment, Individual Support (CEECIND)—5th Edition provided by “FCT—Fundação para a Ciência e Tecnologia”.

• InBridge4EU project funded by the Europe's Rail Joint Undertaking under Horizon Europe research and innovation programme under grant agreement No. 101121765. (Views and opinions expressed are however those of the author(s) only and do not necessarily reflect those of the European Union or Europe's Rail Joint Undertaking. Neither the European Union nor the granting authority can be held responsible for them. The authors would like to apologise for any inconvenience caused.)

• The São Paulo Research Foundation (FAPESP Nos. 2021/12367-2 and 2024/06964-6).

VALE Catedra Under Rail.

Open Access This article is licensed under a Creative Commons Attribution 4.0 International License, which permits use, sharing, adaptation, distribution and reproduction in any medium or format, as long as you give appropriate credit to the original author(s) and the source, provide a link to the Creative Commons licence, and indicate if changes were made. The images or other third party material in this article are included in the article's Creative Commons licence, unless indicated otherwise in a credit line to the material. If material is not included in the article's Creative Commons licence and your intended use is not permitted by statutory regulation or exceeds the permitted use, you will need to obtain permission directly from the copyright holder. To view a copy of this licence, visit http://creativecommons.org/licenses/by/4.0/.

References

1. Cantero D, Arvidsson T, OBrien E et al (2016) Train-track-bridge modelling and review of parameters. Struct Infrastruct Eng 12(9):1051–1064
2. Zhai W, Han Z, Chen Z et al (2019) Train-track-bridge dynamic interaction: a state-of-the-art review. Veh Syst Dyn 57(7):984–1027
3. Li Y, Xiang H, Wang Z et al (2022) A comprehensive review on coupling vibrations of train—bridge systems under external excitations. Railw Eng Sci 30(3):383–401
4. Jin X (2022) Research progress of high-speed wheel-rail relationship. Lubricants 10(10):248
5. Montenegro P, Calçada R (2023) Wheel–rail contact model for railway vehicle-structure interaction applications: development and validation. Railw Eng Sci 31(3):181–206
6. Yang Y, Yau J (2017) Resonance of high-speed trains moving over a series of simple or continuous beams with non-ballasted tracks. Eng Struct 143:295–305
7. Ribeiro D, Costa B, Cruz L et al (2021) Simulation of the dynamic behavior of a centenary metallic bridge under metro traffic actions based on advanced interaction models. Int J Str Stab Dyn 21(04):2150057
8. Arvidsson T, Andersson A, Karoumi R (2019) Train running safety on non-ballasted bridges. Int J Rail Transp 7(1):1–22
9. Ma L, Zhang W, Cai SC et al (2021) The dynamic amplification factors for continuous beam bridges along high-speed railways. Adv Struct Eng 24(11):2542–2554
10. Stoura CD, Dimitrakopoulos EG (2020) Additional damping effect on bridges because of vehicle-bridge interaction. J Sound Vib 476:115294
11. Wang L, Zhang X, Liu H et al (2022) Global reliability analysis of running safety of a train traversing a bridge under crosswinds. J Wind Eng Ind Aerodyn 224:104979
12. Montenegro P, Carvalho H, Ortega M et al (2022) Impact of the train-track-bridge system characteristics in the runnability of high-speed trains against crosswinds — part i: Running safety. J Wind Eng Ind Aerodyn 224:104974
13. Gong W, Zhu Z, Liu Y et al (2020) Running safety assessment of a train traversing a three-tower cable-stayed bridge under spatially varying ground motion. Railw Eng Sci 28:184–198
14. Zhao H, Gao L, Wei B et al (2024) Seismic safety assessment with non-gaussian random processes for train-bridge coupled systems. Earthq Eng Eng Vib 23(1):241–260
15. Giannakos K (2012) Comparison of magnitude of actions on track in high-speed and heavy-haul railroads: Influence of resilient fastenings. Transp Res Rec J Transp Res Board 2289(1):70–77
16. Esveld C (2001) Modern railway track, 2nd edn. MRT Productions, Albuquerque
17. Li D, Hyslip J, Sussmann T et al (2015) Railway geotechnics, 1st edn. CRC Press, London
18. Selig ET, Waters JM (1994) Track geotechnology and substructure management. Emerald Publishing Limited, Leeds
19. El-Sibaie M (1863) Zhang YJ (2004) Objective track quality indices. Transp Res Rec J Transp Res Board 1:81–87
20. Zhao J, Chan AHC, Stirling AB et al (2006) Optimizing policies of railway ballast tamping and renewal. Transp Res Rec J Transp Res Board 1943(1):50–56
21. International Union of Railways (2005) Testing and approval of railway vehicles from the point of view of their dynamic behaviour: safety, track fatigue and ride quality. Leaflet 518 (English version), Paris
22. International Union of Railways (2008) Best practice guide for optimum track geometry durability. Paris
23. Andrade AR, Teixeira PF (2012) A bayesian model to assess rail track geometry degradation through its life-cycle. Res Transp Econ 36(1):1–8
24. International Union of Railways (2009) Classification of lines for the purpose of track maintenance. Leaflet 714 (4th ed.), Paris
25. Ticona Melo LR, Bittencourt TN, Ribeiro D et al (2018) Dynamic response of a railway bridge to heavy axle-load trains considering vehicle-bridge interaction. Int J Str Stab Dyn 18(01):1850010
26. Xiao Y, Luo X, Liu J et al (2020) Dynamic response of railway bridges under heavy-haul freight trains. Adv Civ Eng 2020:7486904
27. Neves S, Montenegro P, Azevedo A et al (2014) A direct method for analyzing the nonlinear vehicle-structure interaction. Eng Struct 69:83–89
28. Montenegro P, Neves S, Calçada R et al (2015) Wheel-rail contact formulation for analyzing the lateral train-structure dynamic interaction. Comput Struct 152:200–214
29. Hertz H (1882) Ueber die berührung fester elastischer körper. Journal für die reine und angewandte Mathematik 92:156–171
30. Kalker J (1979) The computation of three-dimensional rolling contact with dry friction. Numerical Meth Engineering 14(9):1293–1307
31. Kalker JJ (1996) Book of tables for the Herzian creep-force law. Delft University of Technology, Faculty of Technical Mathematics and Informatics
32. Montenegro P, Carvalho H, Ribeiro D et al (2021) Assessment of train running safety on bridges: A literature review. Eng Struct 241:112425
33. Nadal J (1908) Locomotives a Vapeur. Éditions Le Vieil Armand, Strasbourg
34. Prud'homme A (1967) La résistance de la voie aux efforts transversaux éxercés par le material roulant. Rev Gen Chem Fer (Revue Generale des Chemins de Fer) 86(1):1–23
35. The European Committee for Standardization (2022) Railway applications. aerodynamics requirements and test procedures for cross wind assessment EN 14067-6:2018+a1:2022. Brussels
36. The European Committee for Standardization (2016) Railway applications — testing and simulation for the acceptance of

running of railway vehicles – running behaviour and stationary tests EN 14363:2016. Brussels
37. The Association of American Railroads (2023) Manual of standards and recommended practices: Section c, part ii - design, fabrication, and construction of freight cars. Washington, DC
38. Ishida H, Matsuo M (1999) Safety criteria for evaluation of railway vehicle derailment. QR RTRI 40(1):18–25
39. Ishida H, Matsuo M, Fujioka T (2007) Safety assessment method of railway vehicle under oscillatory wheel load fluctuation. J Environ Eng 2(2):407–418
40. Montenegro PA (2015) A methodology for the assessment of the train running safety on bridges. Dissertation, Faculdade de Engenharia da Universidade do Porto
41. The European Committee for Standardization (2005) Eurocode: Basis of Structural Design EN 1990
42. The Commission of the European Communities (2002) Commission decision of 30 may 2002 concerning the technical specification for interoperability relating to the infrastructure subsystem of the trans-european high-speed rail system referred to in article 6(1) of council directive 96/48/EC. Official Journal of the European Union
43. Zhai W, Wang K, Cai C (2009) Fundamentals of vehicle–track coupled dynamics. Veh Syst Dyn 47(11):1349–1376
44. Hu B, Schiehlen W (1997) On the simulation of stochastic processes by spectral representation. Probab Eng Mech 12(2):105–113
45. Spiryagin M, Wolfs P, Cole C et al (2016) Design and simulation of heavy haul locomotives and trains. CRC Press
46. Lima E, Baruffaldi L, Manetti J et al (2022) Effect of truck shear pads on the dynamic behaviour of heavy haul railway cars. Veh Syst Dyn 60(4):1188–1208
47. dos Santos GM, Lopes LS, Kina EJ et al (2010) The influence of wheel profile on the safety index. Proc Inst Mech Eng Part F J Rail Rapid Transit 224(5):429–434
48. Bragança C, Neto J, Pinto N et al (2022) Calibration and validation of a freight wagon dynamic model in operating conditions based on limited experimental data. Veh Syst Dyn 60(9):3024–3050